Journal of Mathematical Chemistry Vol. 31, No. 1, January 2002 (© 2002)

Nodal surface approximations to the zero equipotential surfaces for cubic lattices

Paul J.F. Gandy and Jacek Klinowski

Department of Chemistry, University of Cambridge, Lensfield Road, Cambridge CB2 1EW, UK

Received 17 July 2001

Models of electrostatic surfaces in atomic crystals rely on equations involving the Jacobi theta functions. Numerical integration of these is prohibitively time consuming, making it difficult to examine the properties of the fields which give rise to the surfaces. We give simple expressions for the key electrostatic surfaces using Fourier expansions in basis sets of nodal surfaces. Any surface may be computed in seconds in a form ammenable to further analysis. The distribution of the mean and Gaussian curvatures over each surface has been visualised by assigning colours so that the range from minimum to maximum value spans blue to red. We similarly explore the mean and Gaussian scalar fields over a range of triply periodic surfaces of the same morphology.

KEY WORDS: equipotential surfaces, nodal surfaces, triply periodic minimal surfaces, mean curvature, Gaussian curvature

1. Introduction

While conventional crystallography considers atoms to lie in planes which intersect in straight lines, description using two-dimensional surfaces embedded in three-dimensional space has become increasingly important in structural chemistry [1,2]. Different atomic arrangements in solids at varying levels of complexity strongly resemble the geometry of triply periodic minimal surfaces (TPMS), where the mean curvature, $H = (k_1 + k_2)/2$, is zero at every point and k_1 and k_2 are the principal curvatures. Many structures can be described in terms of curved nets folded onto periodic minimal surfaces [3,4]. Triply periodic surfaces can be nodal [5], equipotential [6] or minimal [7–10].

A zero potential surface (ZEPS) separates the positive and negative charges. Von Schnering and Nesper [11] and Barnes [12] represented the zero equipotential in an ionic crystal by the periodic nodal surface corresponding to a small number of Fourier terms. They gave approximate but simple expressions for the zero equipotential surfaces purely with reference to the reciprocal space term. They concluded that the ZEPS are not the same as the TPMS, although they resemble them very closely [13,14]. For example, in CsCl the ZEPS is close to the P surface. To distinguish ZEPS from TPMS of similar

0259-9791/02/0100-0001/0

topology, the names of ZEPS carry an asterisk. The calculation of the potential in an infinite lattice of charges is difficult, because the result involves non-convergent series which also depend on the kind of surface. Ewald [15] and Bertaut [16] calculated Madelung constants for the charge distributions in ionic crystals using Jacobi's theta functions. We have extended this approach [6] to calculate the coordinates of equipotential surfaces. The aim of this paper is to consider the representation of the exact results by sums of Fourier terms for cubic ZEPS in terms of the conventional treatment by Ewald [15] and Bertaut [16,17].

A structure can be considered in terms of a hyperbolic surface by treating a crystal in terms of a periodically varying electric field described by a field vector at all points in three-dimensional space. The atoms are the point singularities of the field, and are considered as zero-dimensional. The conventional concept of chemical bonds is defined by the trajectories within the electric field which link the atoms, and are one-dimensional. By extending the dimensionality we may define a two-dimensional surface to describe the crystal. The hyperbolic geometry of this surface is a natural consequence of describing extended framework structures which are unbounded in any direction.

Not only do ZEPS find close relationships with chemical structures as space descriptors, they also represent definite physical quantities which contain a variety of interactions. For example, the connection between hyperbolic surfaces and crystalline arrays explains the ionic conduction in solid electrolytes, where the motion of the ions proceeds along the tangential fields of minimal surfaces [18]. For example, the solid electrolyte α-AgI has a mobile cation distribution, with the anions frozen in a body-centred cubic lattice. The Ag^+ ions diffuse along the tangential field of the P^* surface created by the array of iodide ions [19]. This is because the largest electric field gradients felt by a positive charged particle on a ZEPS are always perpendicular to the surface and point in the direction of the anions. The high conductivity of the solid electrolyte β-PbF_2 is caused by the highly mobile fluoride ions within the f.c.c. lead matrix, and the T minimal surface closely describes the trajectories of the conducting species [4,20].

The coordinates of the equipotential surface can be expressed in terms of the Jacobi ϑ functions [6]. With $q = e^{\pi i \tau}$, their limiting forms as $\tau \to 0$ are periodic delta functions

$$\vartheta_1(2\pi z, 1) = 2\sum_{n=0}^{\infty}(-1)^n \sin\big[(2n+1)2\pi z\big]$$

$$= -\sum_{-\infty}^{\infty}\left[\delta\left(z-\left(m-\frac{1}{4}\right)\right)-\frac{1}{2}\delta\left(z-\frac{m}{2}\right)\right],$$

$$\vartheta_2(2\pi z, 1) = 2\sum_{n=0}^{\infty}\big[(2n+1)2\pi z\big] = \sum_{m=0}^{\infty}\left[\delta(z-m)-\frac{1}{2}\delta\left(z-\frac{m}{2}\right)\right],$$

$$\vartheta_3(2\pi z, 1) = \sum_{m=-\infty}^{\infty} \mathrm{e}^{4n\pi \mathrm{i} z} = \frac{1}{2} \sum_{-\infty}^{\infty} \delta\left(z - \frac{m}{2}\right),$$

$$\vartheta_4(2\pi z, 1) = \frac{1}{2} \sum_{-\infty}^{\infty} \delta\left[z - \left(\frac{m}{2} - \frac{1}{4}\right)\right].$$

These are the source functions for any electrostatic array of charges with crystallographic symmetry. The electrostatic potential associated with a lattice, the "Ewald sum", is an integral over products of the four theta functions in appropriate combinations to allow overall charge neutrality. For example, the electrostatic potential $V(x, y, z)$ within the CsCl lattice which mimics the P triply periodic minimal surface is proportional to $\int_0^\infty t \, \mathrm{d}t \, (\vartheta_3\vartheta_3\vartheta_3 - \vartheta_4\vartheta_4\vartheta_4)$, where the arguments of the theta functions are πx, πy and πz, and $q \equiv \exp(-t^2)$.

Potentials for the Bravais lattices which mimic the P, C(P), D, G and I-WP surfaces together with their periodic density functions have been calculated [6], but computation involving theta function surfaces is extremely time consuming. We suggest an alternative and much more accessible approach: representation of the exact results by sums of Fourier terms [5]. This enables convenient examination of metric properties.

2. The geometry of zero equipotential surfaces

A ZEPS is triply periodic, has a three-dimensional Bravais lattice and separates space into two interpenetrating labyrinths of positive and negative potential. These do not intersect, except where the potential is zero. ZEPS may be *balanced* (the P*, D*, G* and C(P)* surfaces), which interchange the partial sub-spaces which they divide, and *unbalanced* (the I-WP* surface), which do not. Interchanging positive and negative charges maps $V(\mathbf{r})$ into $-V(\mathbf{r})$. If a ZEPS is balanced, then the Euclidean operation α which interchanges the two labyrinths will have the same effect, $V(\alpha\mathbf{r}) = -V(\mathbf{r})$. Space group symmetry maps one labyrinth into another, but does not change the sign of the potential. When a Euclidean operation is combined with a permutation, *colour symmetry* arises. For ZEPS we only have two regions, one of positive potential and one of negative potential, and the problem of colour symmetry reduces to the simple case of *black and white symmetry* [21]. If we colour regions of positive and negative potential black and white respectively, the two sides of the ZEPS are coloured oppositely and the surface is said to be *oriented*. The uncoloured surface is said to be *unoriented*. Any ZEPS is characterised by two space groups: the symmetry group $\mathcal{G}$ of the surface and the symmetry group $\mathcal{H}$ of a single labyrinth. $\mathcal{H}$ is a subgroup of $\mathcal{G}$ of index 2. Any transformation belonging to $\mathcal{G}$ but not to $\mathcal{H}$, interchanges the two labyrinths. In other words, the uncoloured surface has space group $\mathcal{G}$, and all Euclidean symmetry operations not interchanging the two labyrinths form a sub-group $\mathcal{H}$ of $\mathcal{G}$, of index 2. $\mathcal{H}$ is, therefore, the space group of the coloured surface. The quotient group is isomorphic to the cyclic group of order 2, i.e., $\mathcal{G}/\mathcal{H} \cong \mathcal{Z}_2 \cong \{1, \alpha\}$. For the ZEPS of the CsCl lattice $\mathcal{H} = \mathrm{Pm\overline{3}m}$ (No. 221) and $\mathcal{G} = \mathrm{Im\overline{3}m}$ (No. 229).

For a balanced ZEPS to be non self-intersecting certain symmetry constraints apply for the extension from $\mathcal{H}$ to $\mathcal{G}$. For example, if α is a rotation, it has to be twofold. Koch and Fischer [22] investigated the 1156 group–subgroup pairs to determine which pairs are not incompatible with the existence of a balanced surface free of self-intersections, published a complete list of 547 $\{\mathcal{G}, \mathcal{H}\}$ pairs and deduced the existence of a balanced surface for all but 23 of them. The remaining 23 pairs were deduced by Lord [23].

3. Periodic nodal surfaces

The ZEPS, as well as other periodic surfaces such as TPMS and Fermi surfaces [24], can be approximated by a periodic nodal surface defined by $\Psi(\mathbf{r}) = 0$, for $\Psi(\mathbf{r})$ given in terms of the Fourier series [25]

$$\Psi(\mathbf{r}) = \sum_{\mathbf{k}} \psi_{\mathbf{k}} \mathrm{e}^{\mathrm{i}\mathbf{k}\cdot\mathbf{r}}, \tag{1}$$

where $\mathbf{k}$ are the reciprocal lattice vectors for a given lattice and $\psi_{\mathbf{k}}$ is the complex Fourier amplitude associated with each $\mathbf{k}$-vector. The set of $\psi_{\mathbf{k}}$ over all $\mathbf{k}$ may not necessarily be independent. We require the scalar field $\Psi(\mathbf{r})$ to be real, and hence $\psi_{\mathbf{k}}^* = \psi_{-\mathbf{k}}$. Writing $\psi_{\mathbf{k}} = \alpha_{\mathbf{k}} - \mathrm{i}\beta_{\mathbf{k}}$, our Fourier series becomes

$$\Psi(\mathbf{r}) = \sum_{\mathbf{k}} \big\{ \alpha_{\mathbf{k}} \cos(\mathbf{k}\cdot\mathbf{r}) + \beta_{\mathbf{k}} \sin(\mathbf{k}\cdot\mathbf{r}) \big\}, \tag{2}$$

where $\alpha_{\mathbf{k}}$ and $\beta_{\mathbf{k}}$ are both real, such that

$$\alpha_{\mathbf{k}} = \frac{1}{V} \int \mathrm{d}\mathbf{r}\, \Psi(\mathbf{r}) \cos(\mathbf{k}\cdot\mathbf{r}) \quad \text{and} \quad \beta_{\mathbf{k}} = \frac{1}{V} \int \mathrm{d}\mathbf{r}\, \Psi(\mathbf{r}) \sin(\mathbf{k}\cdot\mathbf{r}),$$

and the integration runs over the unit cell of volume V. Thus, for even functions $\Psi(\mathbf{r})$, $\beta_{\mathbf{k}} = 0\ \forall \mathbf{k}$, and for odd functions, $\alpha_{\mathbf{k}} = 0\ \forall \mathbf{k}$.

For balanced surfaces, we need a Fourier expansion for the space group $\mathcal{H}$, modulated by restrictions imposed by the black and white symmetry. For non-balanced surfaces there is no colour symmetry and we need only consider the space group $\mathcal{H} \equiv \mathcal{G}$. It is well known how to choose the Fourier terms for a given space group $\mathcal{H}$ [26]. In cubic systems, the translational properties of $\mathcal{H}$ correspond to one of the three cubic Bravais lattices: primitive cubic (P), body-centred cubic (I) or face-centred cubic (F).

Further restrictions on the Fourier amplitudes $\psi_{\mathbf{k}}$ arise when we consider symmetry operations which are not pure translations. If P is a rotation, inversion or roto-inversion, and $\mathbf{t}$ a translation which does not belong to the Bravais lattice, their combined operation may be given as $\mathbf{r} \rightarrow P\mathbf{r} + \mathbf{t}$, where $\mathbf{t}$ is non-vanishing for screw axes and glide planes. It now follows from equation (1) that $\psi_{P^{-1}\mathbf{k}} = \psi_{\mathbf{k}} \mathrm{e}^{\mathrm{i}\mathbf{k}\cdot\mathbf{t}}$. If H is a point group of the given space group $\mathcal{H}$, then for each operation in H there corresponds a pair $(P, \mathbf{t})$ in $\mathcal{H}$. All reciprocal lattice vectors of the same wavelength related by an operation of H are grouped together. The groups are ordered by decreasing wavelength and numbered with

an index i. For each group we choose one representative $\mathbf{k}_i$. By setting $\psi_{\mathbf{k}_i} = \alpha_i - \mathrm{i}\beta_i$ equation (1) becomes a sum over wavelengths,

$$\Psi(\mathbf{r}) = \sum_i \frac{n_i}{n}\left\{\alpha_i \alpha_{\mathbf{k}_i}(\mathbf{r}) + \beta_i \beta_{\mathbf{k}_i}(\mathbf{r})\right\},$$

where n denotes the order of H and n_i the multiplicity of $\mathbf{k}_i$. The *geometric structure factors* $\alpha_{\mathbf{k}_i}(\mathbf{r})$ and $\beta_{\mathbf{k}_i}(\mathbf{r})$ are defined by

$$\alpha_{\mathbf{k}_i}(\mathbf{r}) = \sum_H \cos\left[\left(P^{-1}\mathbf{k}_i\right)\cdot\mathbf{r} + \mathbf{k}_i\cdot\mathbf{t}\right] \quad \text{and} \quad \beta_{\mathbf{k}_i}(\mathbf{r}) = \sum_H \sin\left[\left(P^{-1}\mathbf{k}_i\right)\cdot\mathbf{r} + \mathbf{k}_i\cdot\mathbf{t}\right]$$

summed over all non-translational symmetry operations of space group $\mathcal{H}$. We also need to account for the multiplicity of the Bravais lattice, m_{L} (1, 2, and 4 for P, I, and F surfaces, respectively) by multiplying each equation by a factor of $1/m_{\mathrm{L}}$. Our results are consistent with [26], which contains their explicit forms.

If H does not contain inversion, then $\psi^*_{\mathbf{k}} = \psi_{-\mathbf{k}}$, and we need to use the *Laue group* instead. We have only considered surfaces with point or Laue group $m\overline{3}m$ (of order $n = 48$). Thus, members of each group of reflection planes of the same wavelength are generated by all possible permutations and changes of sign of the components of $\mathbf{k}_i$. With $\alpha_i = \alpha_{\mathbf{k}_i}$ and $\beta_i = \beta_{\mathbf{k}_i}$, every wavelength has two variables. This reduces to one when Ψ is an even or odd function of $\mathbf{r}$.

We must now include the additional black and white symmetry. $\mathcal{H}$ has index 2 in $\mathcal{G}$, and therefore, $\mathcal{H}$ has either the same point group or the same Bravais lattice as $\mathcal{G}$ by Hermann's theorem [27]. If $\mathcal{H}$ and $\mathcal{G}$ have the same point group, their Bravais lattices must be different. In other words, the Euclidean operation α, which interchanges regions of positive and negative potential, has to be the translation $\mathbf{t}_\alpha$ which transforms one cubic Bravais lattice into another. There are only two possibilities. For $\mathbf{t}_\alpha = a(\mathbf{x}+\mathbf{y}+\mathbf{z})/2$ a P lattice is transformed into an I lattice, and for $\mathbf{t}_\alpha = a\mathbf{x}/2$ an F lattice is transformed into a P lattice. So, for black and white symmetry we require equation (1) to satisfy $\Psi(\mathbf{r}+\mathbf{t}_\alpha) = -\Psi(\mathbf{r})$. This leads to the reflection conditions, $h+k+l = 2n+1$ for P $\rightarrow$ I, and $h, k, l = 2n+1$ for F $\rightarrow$ P. These are additional to the standard reflection conditions for I and F, namely, $h+k+l = 2n$ and $h+k$, $h+l$, $k+l = 2n$, respectively. Therefore, in the case of identical point groups, our expressions for the geometric structure factors, $\alpha_{\mathbf{k}_i}(\mathbf{r})$ and $\beta_{\mathbf{k}_i}(\mathbf{r})$, for space group $\mathcal{H}$ remain the same, but the summation now runs over a reduced set of reflection planes.

Conversely, if $\mathcal{H}$ and $\mathcal{G}$ have the *same* Bravais lattice, their point groups must be different. The Euclidean operation α now has to be the point group operation P_α which extends one cubic point group into another. There are five cubic point groups and six ways to extend one into another. Equation (1) must now satisfy $\Psi(P_\alpha\mathbf{r}) = -\Psi(\mathbf{r})$. We now find $\psi_{P_\alpha^{-1}\mathbf{k}} = -\psi_{\mathbf{k}}\exp(\mathrm{i}\mathbf{k}\cdot\mathbf{t}_\alpha)$, and our reflection planes combine to form new ones. However, in this paper we only deal with P_α as the inversion, and no new terms result, since $\mathbf{t}_\alpha = 0$ and $\alpha_i = 0\ \forall i$. This result also follows from equation (2), as now Ψ is an *odd* function of $\mathbf{r}$. The group-subgroup pairs $\{\mathcal{G}, \mathcal{H}\}$ for the five ZEPS examined in this paper are given in tables 1–4 [28].

Table 1
Parameters used in the nodal approximation to the P* and C(P)* surfaces.

$$\{hkl\} = \cos(hx)[\cos(ky)\cos(lz) + \cos(ly)\cos(kz)] + \cos(hy)[\cos(kz)\cos(lx) + \cos(lz)\cos(kx)] + \cos(hz)[\cos(kx)\cos(ly) + \cos(lx)\cos(ky)].$$

(a) P* zero equipotential surface.

h	k	l	Coefficient
1	0	0	1
1	1	1	0.0900395

Notes:

1. Group–subgroup pairs $\{\mathcal{H}, \mathcal{G}\}$: {Pm$\overline{3}$m (No. 221), Im$\overline{3}$m (No. 229)}.
2. R.m.s. error in $\Omega(\mathbf{r}) = 0.000\,150\,906$.
3. Leading order nodal expression: $\cos(x) + \cos(y) + \cos(z) = 0$.

(b) C(P)* zero equipotential surface.

h	k	l	Coefficient
1	0	0	1
1	1	1	0.415003
2	1	0	−0.0941844
3	0	0	−0.108398
2	2	1	0.0448946
3	1	1	−0.0669443
3	2	0	−0.00768723

Notes:

1. Group–subgroup pairs $\{\mathcal{H}, \mathcal{G}\}$: {Pm$\overline{3}$m (No. 221), Im$\overline{3}$m (No. 229)}.
2. R.m.s. error in $\Omega(\mathbf{r}) = 0.005\,286\,19$.
3. Leading order nodal expression: $\cos(x) + \cos(y) + \cos(z) + 4\cos(x)\cos(y)\cos(z) = 0$.

Von Schnering and Nesper reported that the topology of the ZEPS is satisfactorily reproduced by truncating the Fourier series to leading order of unit amplitude, and gave nodal approximations for 21 surfaces, several of them new [11], but never actually showed the surfaces themselves and did not consider the quality of the nodal approximation. The extent of the deviation of ZEPS from TPMS in terms of mean curvature has not been examined. For balanced structures, the correct black-and-white symmetry must be considered. Often one reflection plane is insufficient to represent the topology correctly, and additional terms were added, whose Fourier amplitudes were adjusted by visual inspection. The relevant nodal approximations are given in tables 1–4. The "leading-term-only" nodal surfaces are neither minimal nor constant-mean-curvature surfaces [13,14]. Although these expressions were derived in the context of ZEPS of ionic crystals, they

Table 2
Parameters used in the nodal approximation to the D(43m)* zero equipotential surface.

$$
\begin{aligned}
\{hkl\} = {} & \cos\Big(lz - \tfrac{k}{4} + \tfrac{h}{4}\Big)\Big(\cos\Big(hx + \tfrac{l}{4} - \tfrac{k}{4}\Big)\cos\Big(ky + \tfrac{h}{4} - \tfrac{l}{4}\Big) + \cos\Big(hy + \tfrac{l}{4} - \tfrac{k}{4}\Big)\cos\Big(kx + \tfrac{h}{4} - \tfrac{l}{4}\Big)\Big) \\
& + \cos\Big(lx - \tfrac{k}{4} + \tfrac{h}{4}\Big)\Big(\cos\Big(hy + \tfrac{l}{4} - \tfrac{k}{4}\Big)\cos\Big(kz + \tfrac{h}{4} - \tfrac{l}{4}\Big) \\
& \qquad + \cos\Big(hz + \tfrac{l}{4} - \tfrac{k}{4}\Big)\cos\Big(ky + \tfrac{h}{4} - \tfrac{l}{4}\Big)\Big) \\
& + \cos\Big(ly - \tfrac{k}{4} + \tfrac{h}{4}\Big)\Big(\cos\Big(hz + \tfrac{l}{4} - \tfrac{k}{4}\Big)\cos\Big(kx + \tfrac{h}{4} - \tfrac{l}{4}\Big) \\
& \qquad + \cos\Big(hx + \tfrac{l}{4} - \tfrac{k}{4}\Big)\cos\Big(kz + \tfrac{h}{4} - \tfrac{l}{4}\Big)\Big) \\
& + \sin\Big(lz - \tfrac{k}{4} + \tfrac{h}{4}\Big)\Big(\sin\Big(hx + \tfrac{l}{4} - \tfrac{k}{4}\Big)\sin\Big(ky + \tfrac{h}{4} - \tfrac{l}{4}\Big) + \sin\Big(hy + \tfrac{l}{4} - \tfrac{k}{4}\Big)\sin\Big(kx + \tfrac{h}{4} - \tfrac{l}{4}\Big)\Big) \\
& + \sin\Big(lx - \tfrac{k}{4} + \tfrac{h}{4}\Big)\Big(\sin\Big(hy + \tfrac{l}{4} - \tfrac{k}{4}\Big)\sin\Big(kz + \tfrac{h}{4} - \tfrac{l}{4}\Big) + \sin\Big(hz + \tfrac{l}{4} - \tfrac{k}{4}\Big)\sin\Big(ky + \tfrac{h}{4} - \tfrac{l}{4}\Big)\Big) \\
& + \sin\Big(ly - \tfrac{k}{4} + \tfrac{h}{4}\Big)\Big(\sin\Big(hz + \tfrac{l}{4} - \tfrac{k}{4}\Big)\sin\Big(kx + \tfrac{h}{4} - \tfrac{l}{4}\Big) + \sin\Big(hx + \tfrac{l}{4} - \tfrac{k}{4}\Big)\sin\Big(kz + \tfrac{h}{4} - \tfrac{l}{4}\Big)\Big).
\end{aligned}
$$

h	k	l	Coefficient
1	1	1	1
3	1	1	−0.0000678019
3	3	1	−0.0703087
5	1	1	−0.0672434

Notes:

1. Group–subgroup pairs $\{\mathcal{H}, \mathcal{G}\}$: {Fd$\bar{3}$m (No. 227), Pn$\bar{3}$m (No. 224)}.

2. R.m.s. error in $\Omega(\mathbf{r}) = 0.002\,275\,7$.

3. Leading order nodal expression: $\cos(x)\cos(y)\cos(z) + \sin(x)\sin(y)\sin(z) = 0$.

were used as approximants to TPMS [12,25]. We will discuss our results numerically for the Fourier series of functions $\Psi(\mathbf{r})$, whose zero contours, $\Psi(\mathbf{r}) = 0$, approximate triply periodic ZEPS, and show that the quality of the approximation varies considerably for different structures.

4. Generation of nodal surfaces

To represent ZEPS in terms of nodal surfaces, we construct the Fourier series for the corresponding space group (tables 1–4), as described above, and terminate it after N terms. The ZEPS becomes a function of the Fourier amplitudes α_i and β_i ($1 \leqslant i \leqslant N$), and a constant mode a_0 in the case of the unbalanced I-WP* surface. We set up the equations,

$$a_0 + a_1\Psi_1(x, y, z) + a_2\Psi_2(x, y, z) + a_3\Psi_3(x, y, z) + \cdots = -\Psi_0(x, y, z),$$

where the largest contributing wave, $\Psi_0(x, y, z)$, is given unit amplitude. This set of equations is then solved by the method of least squares, using the Singular Value De-

Table 3
Parameters used in the nodal approximation to the G* zero equipotential surface.

$$\{hkl\} = \cos\left(\tfrac{h+k+l}{4}\right)\left(\begin{array}{l}\left(\begin{array}{l}\cos\left(hx+\frac{l}{4}\right)\cos\left(ky+\frac{h}{4}\right)\cos\left(lz+\frac{k}{4}\right)\\ +\cos\left(kx+\frac{h}{4}\right)\cos\left(ly+\frac{k}{4}\right)\cos\left(hz+\frac{l}{4}\right)\\ +\cos\left(lx+\frac{k}{4}\right)\cos\left(hy+\frac{l}{4}\right)\cos\left(kz+\frac{h}{4}\right)\end{array}\right)\\ +\cos\left(\frac{h+k+l}{4}\right)\left(\begin{array}{l}\cos\left(kx+\frac{l}{4}\right)\cos\left(hy+\frac{k}{4}\right)\cos\left(lz+\frac{h}{4}\right)\\ +\cos\left(lx+\frac{h}{4}\right)\cos\left(ky+\frac{l}{4}\right)\cos\left(hz+\frac{k}{4}\right)\\ +\cos\left(hx+\frac{k}{4}\right)\cos\left(ly+\frac{h}{4}\right)\cos\left(kz+\frac{l}{4}\right)\end{array}\right)\end{array}\right)$$

$$+\cos\left(\tfrac{h+k+l}{4}\right)\left(\begin{array}{l}\left(\begin{array}{l}\sin\left(hx+\frac{l}{4}\right)\sin\left(ky+\frac{h}{4}\right)\sin\left(lz+\frac{k}{4}\right)\\ +\sin\left(kx+\frac{h}{4}\right)\sin\left(ly+\frac{k}{4}\right)\sin\left(hz+\frac{l}{4}\right)\\ +\sin\left(lx+\frac{k}{4}\right)\sin\left(hy+\frac{l}{4}\right)\sin\left(kz+\frac{h}{4}\right)\end{array}\right)\\ +\sin\left(\frac{h+k+l}{4}\right)\left(\begin{array}{l}\sin\left(kx+\frac{l}{4}\right)\sin\left(hy+\frac{k}{4}\right)\sin\left(lz+\frac{h}{4}\right)\\ +\sin\left(lx+\frac{h}{4}\right)\sin\left(ky+\frac{l}{4}\right)\sin\left(hz+\frac{k}{4}\right)\\ +\sin\left(hx+\frac{k}{4}\right)\sin\left(ly+\frac{h}{4}\right)\sin\left(kz+\frac{l}{4}\right)\end{array}\right)\end{array}\right).$$

h	k	l	Coefficient
1	1	0	1
2	1	1	0.0687671
2	2	0	−0.029709
3	1	0	−0.139898
2	2	2	−0.0209595
3	2	1	0.00771151
4	0	0	0.0194887
4	1	1	−0.00922608
3	3	0	0.0250484
4	2	0	0.0741195
3	3	2	−0.00921454
4	2	2	0.000805376
5	1	0	0.0367546
4	3	1	0.0240312
5	2	1	0.0150712
4	4	0	0.00915939
5	3	0	0.00787973
4	3	3	−0.00316782
4	4	2	−0.0133547
6	1	1	0.00313304

Notes:

1. Group–subgroup pairs $\{\mathcal{H}, \mathcal{G}\}$: $\{I4_132$ (No. 214), $Ia\bar{3}d$ (No. 230)$\}$.
2. R.m.s. error in $\Omega(\mathbf{r}) = 0.078\,309\,8$.
3. Leading order nodal expression: $\sin(x)\cos(y) + \sin(z)\cos(x) + \sin(y)\cos(z) = 0$.

Table 4
Parameters used in the nodal approximation to the I-WP* zero equipotential surface.
Constant $a_0 = 0.0117497$.

$$\{hkl\} = \cos^2\left(\tfrac{h+k+l}{4}\right)\begin{pmatrix}\cos(hx)[\cos(ky)\cos(lz)+\cos(ly)\cos(kz)]\\ +\cos(hy)[\cos(kz)\cos(lx)+\cos(lz)\cos(kx)]\\ +\cos(hz)[\cos(kx)\cos(ly)+\cos(lx)\cos(ky)]\end{pmatrix}.$$

h	k	l	Coefficient
1	1	0	1
0	0	0	0.0704983
2	0	0	0.0174117
2	1	1	0.0244038
2	2	0	0.156935
3	1	0	0.00422427
2	2	2	0.0289824
3	2	1	−0.124163
4	0	0	−0.00564199
4	1	1	−0.0586795
3	3	0	−0.0236504
4	2	0	−0.00856369

Notes:

1. Group–subgroup pairs $\{\mathcal{H}, \mathcal{G}\}$: {Im$\overline{3}$m (No. 229), Im$\overline{3}$m (No. 229)}.
2. R.m.s. error in $\Omega(\mathbf{r}) = 0.005\,053\,22$.
3. Leading order nodal expression: $2[\cos(x)\cos(y)+\cos(z)\cos(x)+\cos(y)\cos(z)] - [\cos(2x)+\cos(2y)+\cos(2z)] = 0$.

composition (SVD) process to ensure stability [29]. The quality of the approximation of a surface by a nodal surface depends on the number of terms, N, in the Fourier series. We test for convergence by increasing N and looking for inflection in the r.m.s. errors. If a profile has converged, the Fourier amplitudes fall off exponentially for large $|\mathbf{k}_i|$.

We have generated nodal expressions for five of the zero equipotential surfaces given by the Jacobi theta function model [6]. Figures 1 and 2 show the $\psi = 0$ isosurfaces of the P*, C(P)*, D*, G* and I-WP* ZEPS in a unit cell embedded within their associated electric fields.

The normalised surface-to-volume ratio, $\mathcal{A}/\mathcal{V}^{2/3}$, was calculated for the fundamental region by tesselating the surface with polygons (table 5). By successively refining the discretisation, we calculate the sum of the surface areas of the polygons (A_M) as a function of their number M, and then extrapolate to $A = A_\infty$ by fitting $A \times M$ to a linear $1/M$ dependence. The Euler characteristic χ was calculated for the fundamental lattice region from the Gauss–Bonnet theorem which gives $\chi = 1/(2\pi)\int \mathrm{d}A\, K$.

The surface area $\mathcal{A}$ of an TPMS cell is often expressed via the dimensionless ratio $\sigma = \mathcal{A}/\mathcal{V}^{2/3}$, where $\mathcal{V}$ is the cell volume. The value of σ is invariant with respect to scaling, but depends on the choice of cell. The scaling invariance comes from the fact

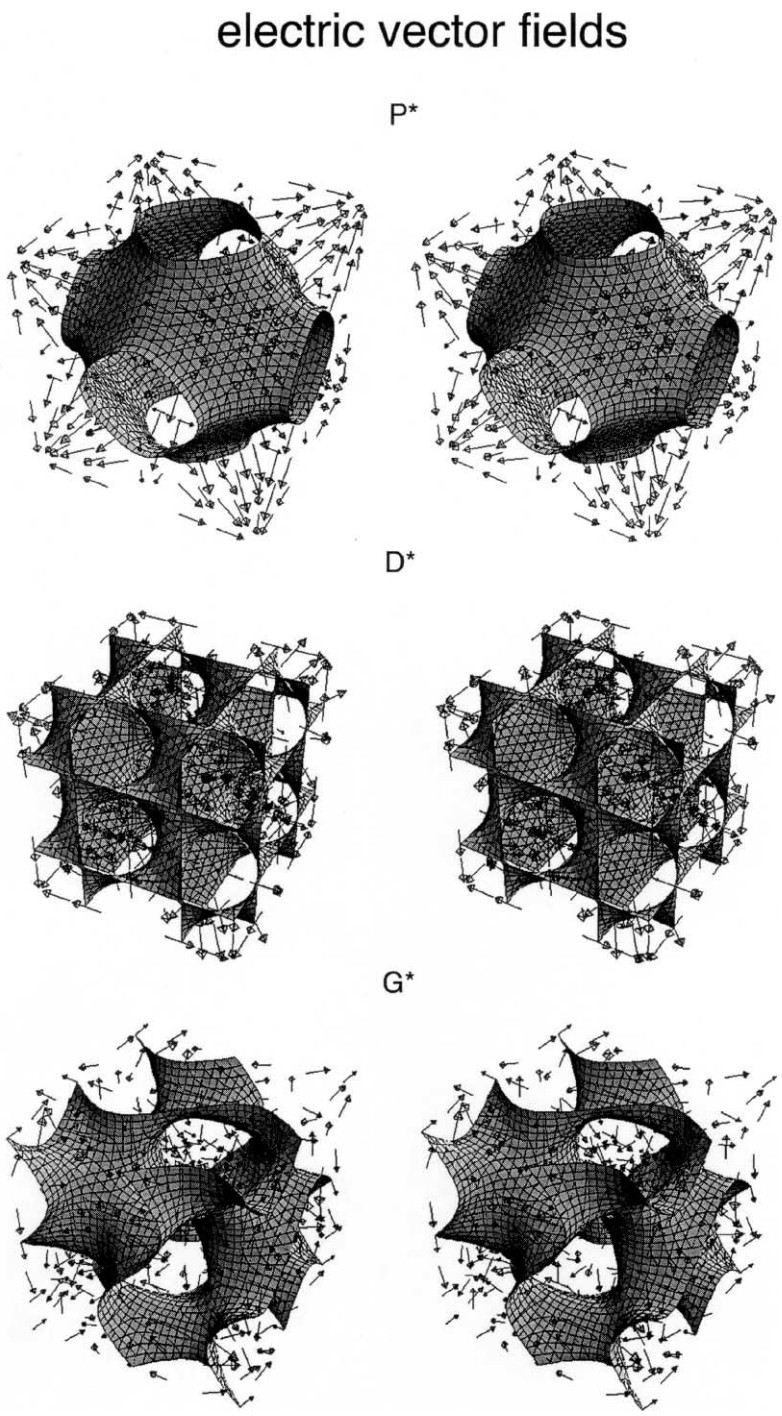

Figure 1. Zero contour plots of P*, D* and G* ZEPS fitted to the nodal surface expressions (tables 1–4) shown as stereo pairs embedded in their respective electric vector fields.

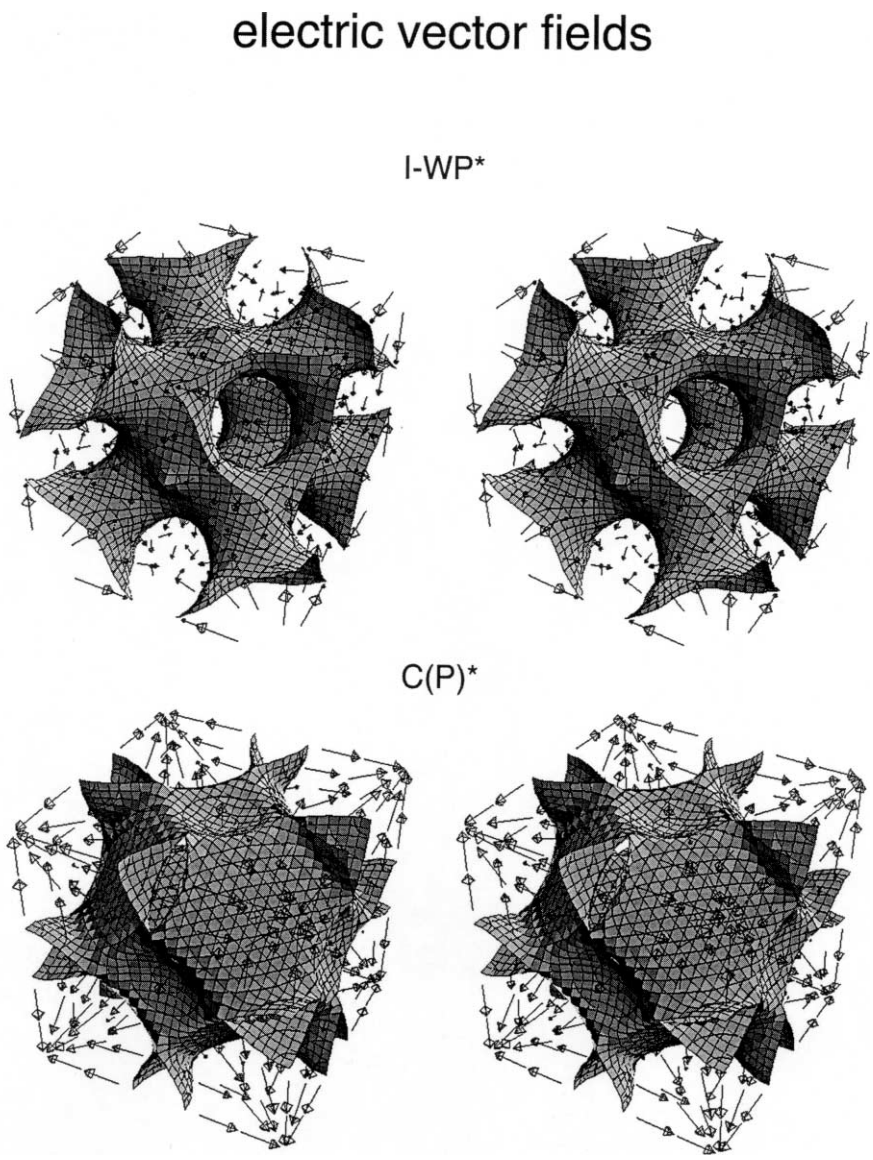

Figure 2. Zero contour plots of I-WP* and C(P)* ZEPS fitted to the nodal surface expressions (tables 1–4) shown as stereo pairs embedded in their respective electric vector fields.

that with a change of length scale by a factor λ, area changes with λ^2 and volume with λ^3. The second property is reflected by the fact that we obtain different dimensionless area figures for the cubic unit cell and the L–F region. Consider two different unit cells, the second containing $k > 0$ copies of the first (k or $1/k$ integer). If the second cell is larger than the first, then $k > 1$. Now σ with respect to the second choice is $(k\mathcal{A})/(k\mathcal{V})^{2/3} = k^{1/3}\mathcal{A}/\mathcal{V}$ in terms of the area and volume of the first choice. Thus, σ scales with $\sqrt[3]{k}$,

Table 5
Metric properties of the P*, D* and G* cubic triply periodic equipotential surfaces within the nodal surface approximation. The table compares the results with those from the leading-order nodal expressions and exact TPMS. $H_{\max}$ is the maximum of $|H|$, $K_{\max}$ is the maximum of $|K|$, and $\langle H^2\rangle = (1/A)\int \mathrm{d}A\, H^2$ is the variance of H over the surface. χ is the Euler characteristic, $\mathcal{A}/\mathcal{V}^{2/3} = \sigma$ is the scaled surface area in the fundamental cell, and $\boldsymbol{H} = (\sigma^3/(2\pi|\chi|))^{1/2}$ is the homogeneity index.

	$H_{\max}$	$\sqrt{\langle H^2\rangle}$	$K_{\max}$	$\mathcal{A}/\mathcal{V}^{2/3}$	χ	$\boldsymbol{H}$
Nodal ZEPS						
P*	2.49	1.07	72.3	2.37	−3.91	0.738
D*	1.94	0.895	66.7	2.42	−15.6	0.761
G*	3.84	1.86	39.7	2.52	−8.01	0.799
0th order nodal						
P	1.29	0.577	39.2	2.35	−3.91	0.729
D	0.387	0.187	39.5	2.42	−15.9	0.755
G	0.209	0.102	29.6	2.45	−7.83	0.775
Nodal TPMS						
P	0.00297	$3.31\cdot10^{-6}$	18.6	2.34	−4.16	0.703
D	0.0410	$1.34\cdot10^{-5}$	45.4	2.42	−15.9	0.753
G	0.00952	$3.03\cdot10^{-6}$	28.2	2.45	−7.78	0.777
Exact TPMS						
P	0	0	18.5	2.34	−4.00	0.716
D	0	0	45.2	2.42	−16.0	0.750
G	0	0	28.1	2.45	−8.00	0.767

and increases for larger unit cells. The dimensionless mean curvature, $H^* = H^3\mathcal{V}^{1/2}$, has the same properties: it is invariant under scaling but changes with $\sqrt[3]{k}$ when a unit cell is replaced by k copies.

It is more convenient to use the so-called homogeneity index $\boldsymbol{H}$ which divides $\sigma^{3/2}$ by $[-2\pi\chi]^{1/2} = [\int(-K)\,\mathrm{d}\mathcal{A}]^{1/2}$, and is, thus, both dimensionless and intensive. $\boldsymbol{H}$ takes the value of 3/4 for a hypothetical minimal surface with uniform K, so its deviation from this "ideality" can give some measure of the inhomogeneity in the Gaussian curvature distribution [14,30].

The mean (H) and Gaussian curvatures (K) are given in terms of the unit electric field vector $\mathbf{E}$ as [31]

$$H = -\nabla\cdot\mathbf{E}$$

and

$$2K = \mathbf{E}\cdot\nabla^2\mathbf{E} + [\nabla\cdot\mathbf{E}]^2 + [\nabla\times\mathbf{E}]^2 = \left[[\nabla\cdot\mathbf{E}]^2 - \sum_{i,j=1}^{3}\partial_i E_j\,\partial_i E_j\right],$$

where $\mathbf{E} = \nabla\Psi/|\nabla\Psi|$ and $\nabla = \mathbf{i}\partial/\partial x + \mathbf{j}\partial/\partial y + \mathbf{k}\partial/\partial z$.

5. Results

We have compared our results for the P*, D* and G* ZEPS with their corresponding TPMS and leading order nodal approximations [8–10]. The Gaussian curvatures of the TPMS (table 5) were calculated from the Weierstrass representation. We evaluated K on a square lattice which covers the fundamental domains for the P, D and G surfaces, and assigned weights to their values. The resulting distributions of H and K were normalised to $\int \mathrm{d}K\, \rho(K) = 1$. For the P, D and G surfaces, the distributions $\rho(K)$ are identical (apart from the scale), since the surfaces are related by the Bonnet transformation.

The nodal representations of ZEPS are plotted as tessellating polygons. We have concentrated on the P*, D* and G* surfaces, as the most frequently occurring in atomic crystals. We have calculated the unit electric field vector normal to each polygon at its centre of gravity, and plotted the result as a three-dimensional vector field over the surfaces (figure 1). The distribution of H and K over each surface has been visualised by assigning a colour to each polygon (figures 3 and 4). Colours of the visible spectrum were assigned numerical values from 0 to 1 cyclically and scaled so that the range from minimum to maximum of H and K spans blue to red. The colouring enables instant comparisons to be made between the surfaces. Table 5 compares the fitted nodal expressions to ZEPS, the leading order nodal approximations and the exact Weierstrass representations by monitoring $H_{\max}$, the maximum of $|H|$ on the surface, $\sqrt{\langle H^2 \rangle}$, the square of the variance of H, and $K_{\min}$, the minimal value of K on the surface. For the exact Weierstrass representation, $H_{\max} = \sqrt{\langle H^2 \rangle} = 0$.

6. Discussion

The ZEPS generated in terms of the theta function are not identical, but very close, to TPMS [14]. The distribution of H over each surface is shown in figure 3. Although the average value of the mean curvature vanishes over a unit cell of the lattice, the magnitude of the mean curvature fluctuates over the surface and is distributed symmetrically around $H = 0$. The distribution of Gaussian curvature for each structure is shown in figure 4. The further away from minimality, the larger the extremal value of the Gaussian curvature, $K_{\min}$. The surface area is not very sensitive to the detailed shape of the surfaces and varies within a few percent. The homogeneity index gives a measure of the porosity of the structure (the larger its value, the less porous) and the specific surface area (the larger its value, the more surface area per volume). The gyroid morphology represents an absolute maximum over each family. The Fourier expansion of nodal surfaces yields representations of triply periodic surfaces which are easy to compute and thus straightforward to use in further studies. The quality of the approximation can be judged from the distribution of H and K over the surface. Leading order nodal approximations can be considerably improved by adding just a few more modes. The different amplitudes for corresponding terms arise from the different shapes of the order parameter profile. However, for sharp interfaces, the Fourier amplitudes decay more and more slowly as a function of the wave number $|\mathbf{k}|$.

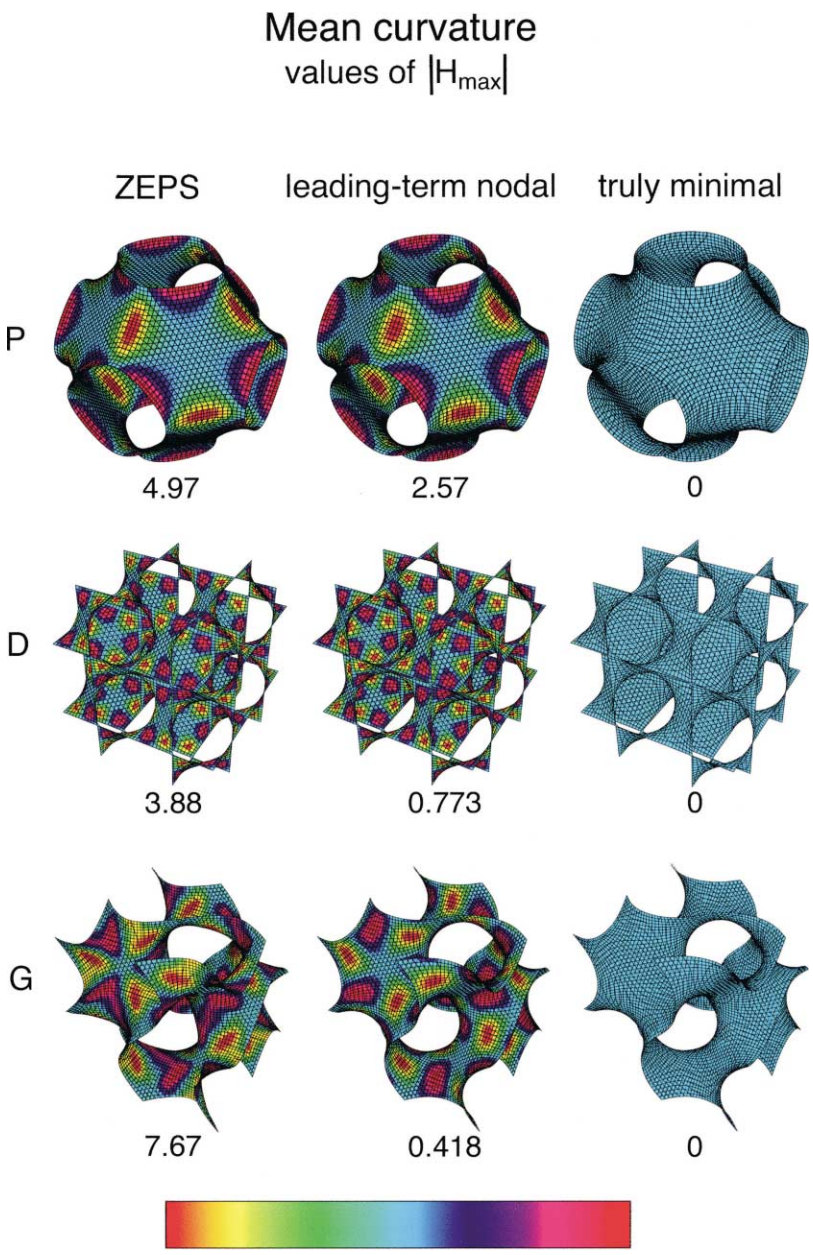

Figure 3. Colour-encoded distribution of the mean curvature, H, shown as ranging from blue ($H_{\min}$) to red ($H_{\max}$) for the P, D and G triply periodic minimal surfaces. The first column shows the distribution of H for the ZEPS approximation, the second for the nodal surface approximation (to leading order), and the third shows H for exact TPMS. The distributions are symmetric about $H = 0$, and numerical values for $H_{\max} = -H_{\min}$ are given in table 5.

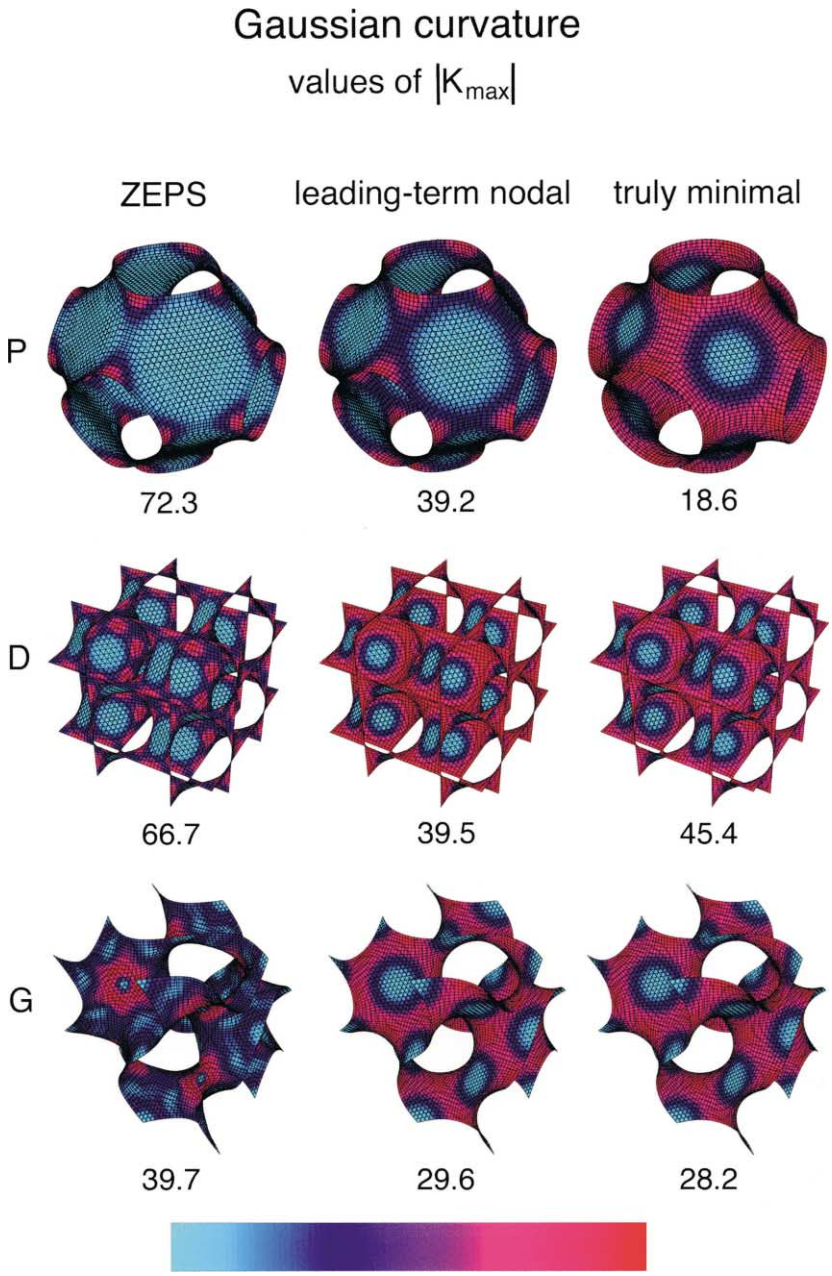

Figure 4. Colour-encoded distribution of the mean curvature, K, shown as ranging from blue ($K_{\min}$) to red ($K_{\max}$) for the P, D and G triply periodic minimal surfaces. The first column shows the distribution of K for the ZEPS approximation, the second for the nodal surface approximation (to leading order), and the third shows K for exact TPMS. The distributions are asymmetric. Numerical values for $K_{\min}$ are given in table 5. For all nine cases $K_{\max} = 0$.

References

[1] S. Andersson, Angew. Chem. Internat. Ed. Engl. 22 (1983) 69.
[2] S. Andersson, S.T. Hyde and H.G. von Schnering, Z. Kristallogr. 168 (1984) 1.
[3] S. Andersson, S.T. Hyde, K. Larsson and S. Lidin, Chem. Rev. 88 (1988) 221.
[4] H.G. von Schnering and R. Nesper, Angew. Chem. Internat. Ed. Engl. 26 (1987) 1059.
[5] P.J.F. Gandy, S. Bardhan, A.L. Mackay and J. Klinowski, Chem. Phys. Lett. 336 (2001) 187.
[6] P.J.F. Gandy and J. Klinowski, Chem. Phys. Lett. (2001) (submitted).
[7] D. Cvijović and J. Klinowski, Chem. Phys. Lett. 226 (1994) 93.
[8] P.J.F. Gandy, D. Cvijović, A.L. Mackay and J. Klinowski, Chem. Phys. Lett. 314 (1999) 543.
[9] P.J.F. Gandy and J. Klinowski, Chem. Phys. Lett. 322 (2000) 579.
[10] P.J.F. Gandy and J. Klinowski, Chem. Phys. Lett. 321 (2000) 363.
[11] H.G. von Schnering and R. Nesper, Z. Phys. B 83 (1991) 407.
[12] I. Barnes, Austral. Math. Soc. Gazette 17 (1990) 99.
[13] A.L. Mackay and J. Klinowski, Comput. Math. Appl. B 12 (1986) 803.
[14] I.S. Barnes, S.T. Hyde and B.W. Ninham, J. Phys. (Paris) 51(C7) (1990) 19.
[15] P.P. Ewald, Ann. Physik IV 64 (1921) 253–287.
[16] F. Bertaut, J. Phys. Radium 13 (1952) 499–505.
[17] F. Bertaut, J. Phys. Chem. Solids 39 (1978) 97.
[18] S. Andersson, S.T. Hyde and J.O. Bovin, Z. Kristallogr. 173 (1985) 97.
[19] R.J. Cava, F. Reidinger and B.J. Wuensch, in: eds. P. Vashishta, J.N. Mundy and G.K. Shenoy, *Fast Ion Transport in Solids* (North Holland, Amsterdam, 1979).
[20] S. Hyde, Philos. Mag. B 57 (1988) 691.
[21] A. L. Loeb, *Color and Symmetry* (Wiley, New York, 1971).
[22] E. Koch and W. Fischer, Z. Kristallogr. 183 (1988) 129.
[23] E.A. Lord, Colloids and Surfaces A 130 (1997) 279.
[24] M.R. Halse, Phil. Trans. Roy. Soc. London Ser. A 265 (1969) 507.
[25] A.L. Mackay, Chem. Phys. Lett. 221 (1994) 317.
[26] K. Lonsdale and N.F.M. Henry (eds.), *International Tables for X-Ray Crystallography*, Vol. 1, Symmetry Groups (Kynoch Press, International Union of Crystallography, Birmingham, 1952).
[27] M. Senechal, *Crystalline Symmetries: An Informal Mathematical Introduction* (Hilger, Bristol, 1990).
[28] W. Fischer and E. Koch, Z. Kristallogr. 179 (1987) 31.
[29] W.H. Press, B.P. Flannery, S.A. Teukolsky and W.T. Vetterling, *Numerical Recipes* (Cambridge University Press, Cambridge, UK, 1986).
[30] S.T. Hyde, Current Opinion in Solid State and Materials Science 1 (1996) 653.
[31] C.E. Weatherburn, *The Differential Geometry of Three Dimensions*, Vol. II (Cambridge University Press, 1930) pp. 85–91.